An Efficient DGTD Implementation of the Uniaxial Perfectly Matched Layer

Da Peng[1], Lin Chen[2], Wenlu Yin[2], Hu Yang[1]
[1]College of Electronic Science and Engineering, National Univ. of Defense Technology
Changsha, Hunan 410073, China
[2]Southwest Electronics and Telecommunication Technology Research Institute
Chengdu, Sichuan 610041, China

***Abstract*- we proposed a straightforward and highly efficient DGTD implementation of the Uniaxial Perfectly Matched Layer (UPML). Discontinuous Galerkin method (DGM) is imposed on both the UPML Maxwell's curl equations and the auxiliary differential equations (ADE). By recording the intermediate results in the updated processes of E-fields and H-fields, the computation time for auxiliary variables in ADE can be reduced greatly within each time step. Moreover, the auxiliary variables and Riemann flux on each elemental interface are treated dependently here, using which, an excellent stable PML scheme can be obtained. Some examples demonstrate the effectiveness of this UPML, and the proposed method behaves much more stable than the well-posed PML, which is commonly used as PML absorber in DGTD algorithm currently.**

I. INTRODUCTION

Discontinuous Galerkin Time-Domain (DGTD) method is a very useful full-wave numerical algorithm to solve large-scale time-dependent electromagnetic problems with complex geometries in which high accuracy and efficiency are required. It employs discontinuous piecewise polynomials as basis and test functions, and then applies a Galerkin test procedure for each element to obtain the spatial discretization. The solution is not enforced continuous across interface of any two adjacent elements. Instead, a unique numerical flux is constructed to provide the coupling mechanism between elements, which gives rise to a highly parallel formulation.

One of the greatest challenges for DGTD has been obtaining the efficient and accurate solution of electromagnetic wave interaction problems in an open region. In general, there are two classes techniques for such problems: analytical absorbing boundary conditions (ABC) and perfectly matched layer (PML). For the former, a first-order Silver-Müller ABC [1] is employed in the early researches, which is equivalent to Shankar et al.'s [2] straightforward approach of setting the incoming flux to zero in Riemann flux, and a high-order ABC [3] is developed subsequently by William F. Hall and Adour V. Kabakian. Such approaches require putting the outer boundary at least a few wavelengths away from the scatterer in order to get reasonable reflections. This condition leads to an increase of the computational domain scale and CPU time. In the latter case, the well-posed PML is adopted for computational domain truncation by Tian Xiao and Qing H. Liu [4]. In [5,6,15], the auxiliary fileds are redesigned to make the curl operator vanish in the auxiliary differential equations (ADE). Unfortunately, these PML suffers from some problems of stability [7] when incorporated with DGTD, especially in the case of existence of some very distorted cells in the PML mesh.

In this paper, we proposed a straightforward and highly efficient DGTD implementation of the Uniaxial Perfectly Matched Layer (UPML). Discontinuous Galerkin method (DGM) is imposed on both the UPML Maxwell's curl equations and the auxiliary differential equations (ADE). In ADE, the auxiliary variables and Riemann flux [8] on each elemental interface are treated dependently, using which, an excellent stable PML scheme can be obtained. Finally, the UPML is validated through some examples. Numerical results show this UPML is effective, and much more stable than the well-posed PML, which is commonly used as PML absorber in DGTD algorithm currently.

II. THEORY

To model electromagnetic waves in an unbounded physical domain, an anisotropic form of the PML [9] is applied here to the DGTD formulation. Maxwell's curl equations are expressed as follows in the PML:

$$\frac{\partial(\mu \boldsymbol{H})}{\partial t} + K(\nabla \times \boldsymbol{E}) = C\boldsymbol{B} - \sigma_m \boldsymbol{H} \tag{1}$$

$$\frac{\partial(\varepsilon \boldsymbol{E})}{\partial t} - K(\nabla \times \boldsymbol{H}) = C\boldsymbol{D} - \sigma \boldsymbol{E} \tag{2}$$

where the diagonal matrices K, C, σ and σ_m are defined as

$$K = Diag\left[\frac{\kappa_x}{\kappa_y\kappa_z}, \frac{\kappa_y}{\kappa_x\kappa_z}, \frac{\kappa_z}{\kappa_x\kappa_y}\right],$$

$$C = \frac{1}{\varepsilon} Diag\left[\frac{\sigma_x}{\kappa_z} - \frac{\kappa_x}{\kappa_y\kappa_z}\sigma_y, \frac{\sigma_y}{\kappa_x} - \frac{\kappa_y}{\kappa_x\kappa_z}\sigma_z, \frac{\sigma_z}{\kappa_y} - \frac{\kappa_z}{\kappa_x\kappa_y}\sigma_x\right],$$

$$\sigma = Diag\left[\frac{\sigma_z}{\kappa_z}, \frac{\sigma_x}{\kappa_x}, \frac{\sigma_y}{\kappa_y}\right],\ \sigma_m = \frac{\mu}{\varepsilon}\sigma,$$

and the flux densities $\boldsymbol{B}$ and $\boldsymbol{D}$ satisfy the following ADE:

$$\frac{\partial(\kappa \boldsymbol{B})}{\partial t} + \nabla \times \boldsymbol{E} = -\gamma \boldsymbol{B} \tag{3}$$

$$\frac{\partial(\kappa \boldsymbol{D})}{\partial t} - \nabla \times \boldsymbol{H} = -\gamma \boldsymbol{D} \tag{4}$$

where

$$\kappa = Diag\left[\kappa_y, \kappa_z, \kappa_x\right], \quad \gamma = \frac{1}{\varepsilon} Diag\left[\sigma_y, \sigma_z, \sigma_x\right].$$

Note that the UPML Maxwell's equations can reduce to the original Maxwell's equations by setting the PML coefficients $\sigma_x = \sigma_y = \sigma_z = 0$ and $\kappa_x = \kappa_y = \kappa_z = 1$. Therefore, in terms of spatial discretization, it permits a unified treatment of both the lossless interior working volume and the UPML slabs.

For the convenience of using DGM, the above equations are written compactly in a conservation form:

$$Q\frac{\partial \boldsymbol{q}}{\partial t} + \tilde{K}\nabla \cdot \boldsymbol{F}(\boldsymbol{q}) = \boldsymbol{f} \tag{5}$$

$$\tilde{\kappa}\frac{\partial \boldsymbol{p}}{\partial t} + \nabla \cdot \boldsymbol{F}(\boldsymbol{q}) = \boldsymbol{g} \tag{6}$$

where the material matrix Q, the state vectors $\boldsymbol{q}$ and $\boldsymbol{p}$, the flux $\boldsymbol{F}(\boldsymbol{q}) = \left[F_x, F_y, F_z\right]^T$, and the body forces $\boldsymbol{f}$, $\boldsymbol{g}$ are defined as follows:

$$Q = \begin{bmatrix} \mu & \\ & \varepsilon \end{bmatrix}, \ \tilde{K} = \begin{bmatrix} K & \\ & K \end{bmatrix}, \ \tilde{\kappa} = \begin{bmatrix} \kappa & \\ & \kappa \end{bmatrix} \tag{7}$$

$$\boldsymbol{q} = \begin{bmatrix} \boldsymbol{H} \\ \boldsymbol{E} \end{bmatrix}, \ \boldsymbol{p} = \begin{bmatrix} \boldsymbol{B} \\ \boldsymbol{D} \end{bmatrix} \tag{8}$$

$$F_i(\boldsymbol{q}) = \begin{bmatrix} e_i \times \boldsymbol{E} \\ -e_i \times \boldsymbol{H} \end{bmatrix} \tag{9}$$

$$\boldsymbol{f} = \begin{bmatrix} C\boldsymbol{B} - \sigma_m \boldsymbol{H} \\ C\boldsymbol{D} - \sigma \boldsymbol{E} \end{bmatrix}, \ \boldsymbol{g} = \begin{bmatrix} -\gamma \boldsymbol{B} \\ -\gamma \boldsymbol{D} \end{bmatrix}. \tag{10}$$

Here, e_i denotes the three Cartesian unit vectors.

The spatial discretization of (5) and (6) is based on a Galerkin discretization procedure for the spatial derivatives. First, the space domain needs to be partitioned into nonoverlapping elements. To capture the complex geometries, an unstructured grid is used to divide the computational domain into a number of tetrahedrons. Then, within each tetrahedral element, the Lagrange interpolation polynomials $L_j(\boldsymbol{x})$, associated with a set of nodal points $\boldsymbol{x}_j$, are chosen for the local basis function sets of order n (we refer to this scheme as DGTD-p_n), and the state vectors $\boldsymbol{q}$ and $\boldsymbol{p}$ can be represented as

$$\boldsymbol{q}(\boldsymbol{x}, t) \approx \sum_{j=1}^{N} \boldsymbol{q}(\boldsymbol{x}_j, t) L_j(\boldsymbol{x}) = \sum_{j=1}^{N} \boldsymbol{q}_j(t) L_j(\boldsymbol{x}) \tag{11}$$

$$\boldsymbol{p}(\boldsymbol{x}, t) \approx \sum_{j=1}^{N} \boldsymbol{p}(\boldsymbol{x}_j, t) L_j(\boldsymbol{x}) = \sum_{j=1}^{N} \boldsymbol{p}_j(t) L_j(\boldsymbol{x}) \tag{12}$$

where N denotes the total number of nodes in a tetrahedron and is equal to $(n+1)(n+2)(n+3)/6$. More details can be found in [10].

The test functions are chosen to be the same as the basis functions. Multiplied by the test functions and integrated over each element, two weak forms of Eqs. (5) and (6) are obtained over each element $\mathbf{D}$

$$\int_{\mathbf{D}} Q\frac{\partial \boldsymbol{q}}{\partial t} L_i(\boldsymbol{x}) d\boldsymbol{x} = -\int_{\mathbf{D}} \tilde{K}\nabla \cdot \boldsymbol{F} L_i(\boldsymbol{x}) d\boldsymbol{x} + \int_{\mathbf{D}} \boldsymbol{f} L_i(\boldsymbol{x}) d\boldsymbol{x}$$

$$\int_{\mathbf{D}} \tilde{\kappa}\frac{\partial \boldsymbol{p}}{\partial t} L_i(\boldsymbol{x}) d\boldsymbol{x} = -\int_{\mathbf{D}} \nabla \cdot \boldsymbol{F} L_i(\boldsymbol{x}) d\boldsymbol{x} + \int_{\mathbf{D}} \boldsymbol{g} L_i(\boldsymbol{x}) d\boldsymbol{x}.$$

Applying the divergence theorem to the first term on the right-hand side, we obtain

$$\begin{aligned} \int_{\mathbf{D}} Q\frac{\partial \boldsymbol{q}}{\partial t} L_i(\boldsymbol{x}) d\boldsymbol{x} &= -\int_{\partial \mathbf{D}} \tilde{K}(\hat{\boldsymbol{n}} \cdot \boldsymbol{F}) L_i(\boldsymbol{x}) d\boldsymbol{x} \\ &\quad + \int_{\mathbf{D}} \tilde{K}\boldsymbol{F} \cdot \nabla L_i(\boldsymbol{x}) d\boldsymbol{x} + \int_{\mathbf{D}} \boldsymbol{f} L_i(\boldsymbol{x}) d\boldsymbol{x} \end{aligned} \tag{13}$$

$$\begin{aligned} \int_{\mathbf{D}} \tilde{\kappa}\frac{\partial \boldsymbol{p}}{\partial t} L_i(\boldsymbol{x}) d\boldsymbol{x} &= -\int_{\partial \mathbf{D}} \hat{\boldsymbol{n}} \cdot \boldsymbol{F} L_i(\boldsymbol{x}) d\boldsymbol{x} \\ &\quad + \int_{\mathbf{D}} \boldsymbol{F} \cdot \nabla L_i(\boldsymbol{x}) d\boldsymbol{x} + \int_{\mathbf{D}} \boldsymbol{g} L_i(\boldsymbol{x}) d\boldsymbol{x} \end{aligned} \tag{14}$$

where $\partial\mathbf{D}$ is the boundary of element $\mathbf{D}$ and $\hat{\boldsymbol{n}}$ is the outward unit normal vector. The Riemann flux $\hat{\boldsymbol{n}} \cdot \boldsymbol{F}$ is obtained by solving exactly the one-dimensional Riemann problem on each elemental interface [8]:

$$\hat{\boldsymbol{n}} \cdot \boldsymbol{F}\big|_{\partial \mathbf{D}} = \begin{bmatrix} \hat{\boldsymbol{n}} \times \dfrac{(Y\boldsymbol{E} - \hat{\boldsymbol{n}} \times \boldsymbol{H})^- + (Y\boldsymbol{E} + \hat{\boldsymbol{n}} \times \boldsymbol{H})^+}{Y^- + Y^+} \\ -\hat{\boldsymbol{n}} \times \dfrac{(Z\boldsymbol{H} + \hat{\boldsymbol{n}} \times \boldsymbol{E})^- + (Z\boldsymbol{H} - \hat{\boldsymbol{n}} \times \boldsymbol{E})^+}{Z^- + Z^+} \end{bmatrix} \tag{15}$$

where Z and Y are the impedance and admittance of the medium respectively. The superscript "-" refers to the outgoing flux and the superscript "+" to the incoming flux across the interface. For the special case of a PEC boundary, the boundary flux can be obtained by setting $Y^+ = \infty$ because the PEC boundary behaves as a material with an infinite admittance. Similarly, a PMC boundary corresponds to the case of setting $Z^+ = \infty$. As for the absorbing boundary, a straightforward approach of setting the incoming flux to zero is employed [2,11].

Substituting Eqs. (7)~(12) into Eqs. (13) and (14), and on the assumption that ε, μ are elementwise constant, we obtain the semi-discrete scheme in a matrix form

$$\frac{\partial \mathbf{H}}{\partial t} = \frac{1}{\mu}\left(-\mathbf{M}^{-1}\sum_{m=1}^{4} \mathbf{F}^m \left[K\hat{\mathbf{n}} \times \frac{(Y\mathbf{E} - \hat{\mathbf{n}} \times \mathbf{H})^- + (Y\mathbf{E} + \hat{\mathbf{n}} \times \mathbf{H})^+}{Y^- + Y^+} \right]_{\partial \mathbf{D}_m} + \mathbf{M}^{-1} K\mathbf{S} \times \mathbf{E} + \left[C\mathbf{B} - \sigma_m \mathbf{H} \right] \right) \tag{16}$$

$$\frac{\partial \mathbf{E}}{\partial t} = \frac{1}{\varepsilon}\left(\mathbf{M}^{-1}\sum_{m=1}^{4} \mathbf{F}^m \left[K\hat{\mathbf{n}} \times \frac{(Z\mathbf{H} + \hat{\mathbf{n}} \times \mathbf{E})^- + (Z\mathbf{H} - \hat{\mathbf{n}} \times \mathbf{E})^+}{Z^- + Z^+} \right]_{\partial \mathbf{D}_m} - \mathbf{M}^{-1} K\mathbf{S} \times \mathbf{H} + \left[C\mathbf{D} - \sigma \mathbf{E} \right] \right) \tag{17}$$

$$\kappa\frac{\partial \mathbf{B}}{\partial t} = -\mathbf{M}^{-1}\sum_{m=1}^{4} \mathbf{F}^m \left[\hat{\mathbf{n}} \times \frac{(Y\mathbf{E} - \hat{\mathbf{n}} \times \mathbf{H})^- + (Y\mathbf{E} + \hat{\mathbf{n}} \times \mathbf{H})^+}{Y^- + Y^+} \right]_{\partial \mathbf{D}_m} + \mathbf{M}^{-1}\mathbf{S} \times \mathbf{E} - \gamma \mathbf{B} \tag{18}$$

$$\kappa\frac{\partial \mathbf{D}}{\partial t} = \mathbf{M}^{-1}\sum_{m=1}^{4} \mathbf{F}^m \left[\hat{\mathbf{n}} \times \frac{(Z\mathbf{H} + \hat{\mathbf{n}} \times \mathbf{E})^- + (Z\mathbf{H} - \hat{\mathbf{n}} \times \mathbf{E})^+}{Z^- + Z^+} \right]_{\partial \mathbf{D}_m} - \mathbf{M}^{-1}\mathbf{S} \times \mathbf{H} - \gamma \mathbf{D}. \tag{19}$$

Here we have

$$\mathbf{M}_{ij} = \int_{\mathbf{D}} L_i(\boldsymbol{x}) L_j(\boldsymbol{x}) d\boldsymbol{x}, \ \mathbf{S}_{ij} = \int_{\mathbf{D}} \nabla L_i(\boldsymbol{x}) L_j(\boldsymbol{x}) d\boldsymbol{x},$$

$$\mathbf{F}_{ij}^m = \int_{\partial \mathbf{D}_m} L_i(\boldsymbol{x}) L_j(\boldsymbol{x}) d\boldsymbol{x}$$

and $\mathbf{H}$, $\mathbf{E}$, $\mathbf{B}$, $\mathbf{D}$ are vectors whose entries associate with corresponding nodes. Note that there is a similarity between (16) and (18), (17) and (19). By recording the intermediate

results in the updated processes of **H** and **E**, the computation time for **B** and **D** can be reduced greatly, which brings an efficient implementation. Moreover, the auxiliary variables of **B** and **D** are dependent with Riemann flux on each elemental interface. It leads to an excellent stable PML scheme.

Following the spatial discretization, we use an explicit time integration scheme, namely a 2th-order two-stage Runge-Kutta low-storage method. The scheme to solve equation, $d\mathbf{U}/dt = R(t,\mathbf{U})$, is represented as [12]

$$\left.\begin{aligned} \mathbf{Q}^0 &= \mathbf{U}^n \\ k_j &= a_j k_{j-1} + \Delta t \cdot R\left(\left(n + c_j\right)\Delta t, \mathbf{Q}^{j-1}\right) \\ \mathbf{Q}^j &= \mathbf{Q}^{j-1} + b_j k_{j-1} \end{aligned}\right\} \forall j \in [1,2] \qquad (20)$$
$$\mathbf{U}^{n+1} = \mathbf{Q}^2$$

where $a_1 = c_1 = 0$, $b_1 = c_2 = 0.5$, $a_2 = -0.5$, and $b_2 = 1$.

III. Numerical Results

Because the convergence of DGTD with a set of fixed grids by increasing the order of the approximation within each tetrahedron is beyond our discussion in this paper, unless stated otherwise, all examples are done using a second-order scheme (DGTD-p_2) and an average element size of $\lambda/4$ is adopted for tetrahedron mesh generation.

To demonstrate the effectiveness of UPML as an ABC, the radiation of current source in an unbounded 3D region is considered firstly. As shown in Figure 1, an electric current source **J** is surrounded by the air with PML as the outer boundary condition and has the time signature of a differentiated Gaussian pulse

$$J_z = -2\left[(t-t_0)/\tau\right]\exp\left\{-\left[(t-t_0)/\tau\right]^2\right\} \qquad (21)$$

where $\tau = 1.25ns$ and $t_0 = 4.5\tau$.

The finite element grids consist of 22867 tetrahedrons with an average element size of 0.25m. The component E_z is probed at two points, A and B, as shown in the Figure 1. A relative error is defined as

$$Rel.error\big|_{(x,y,z)}^{n\Delta t} = 20\log_{10}\left(\left|E^{n\Delta t} - E_{ref}^{n\Delta t}\right| / \left|E_{ref\ max}\right|\right)\Big|_{(x,y,z)} \quad (dB) \qquad (22)$$

where $E_{ref\ max}$ is the maximum amplitude of the reference field obtained at spatial location (x,y,z) by running a sufficiently large grids. Figure 2 graphs the relative error calculated using (22) at points A and B. Here, the key UPML parameters [14] are $\sigma_{max} = \sigma_{opt}$, $\kappa_{max} = 1$ and $m = 4$. The perpendicular reflection error is set as $R(0) = e^{-8}$.

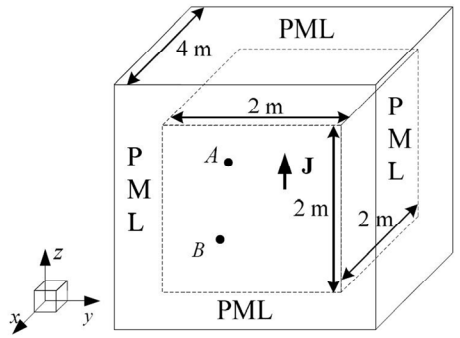

Figure 1. z-directed electric current source located at (0.023, -0.134, 0.016 m) in a 3-D DGTD grid. E-fields are probed at points A (0.122, -0.16, -0.66 m) and B (-0.147, 0.575, -0.664 m)

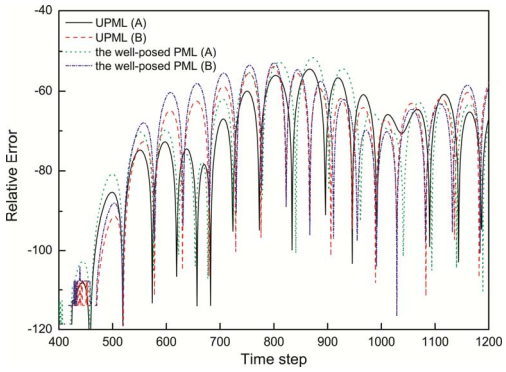

Figure 2. Relative error at points A and B of Fig. 1 over 1200 time-steps for two PML approaches

From this example, it was observed that UPML has a reflection error comparable to or even better than the well-posed PML for the outgoing waves absorption.

Subsequently, let us consider plane wave scattering by perfectly conducting sphere, the analytic solution of which is given by a Mie series. We use both the well-posed PML and the UPML to truncate the computational domain for the same finite element discretization, and choose the PML parameters for the former as recommended in [13]. The thickness of perfectly matched layer is set to half a wavelength.

The perfectly conducting sphere with a diameter of 15λ is illuminated by a Gaussian derivative pulse whose waveform is depicted by (21), and the component E_z is probed at the same position for both PML approaches. The received signal becomes unstable after 4300 time steps when using the well-posed PML (Figure 4(a)), whereas no sign of instability is observed after 8000 time steps for UPML. The E-plane bistatic cross sections are shown in Figure 4(b). It is in good agreement with the exact solution. The finite element grids consist of 807950 tetrahedrons (Figure 3), and a memory size of 1.53G Bytes is required.

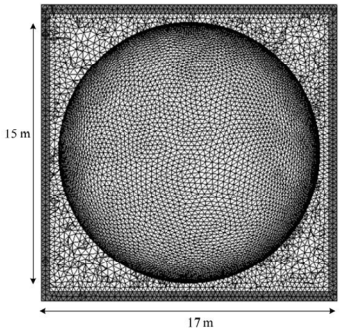

Figure 3. The finite element grid, consisting of 807950 tetrahedrons, used for computing scattering by a PEC sphere with a diameter of 15λ

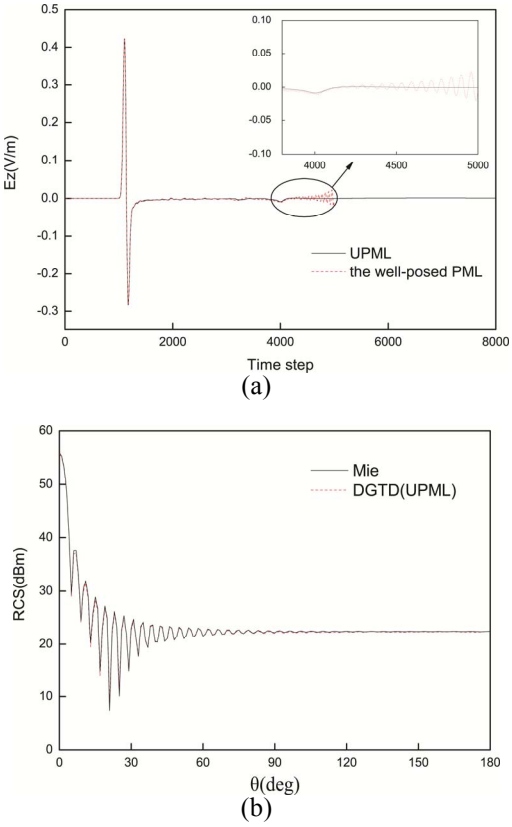

Figure 4. (a) Comparison of E_z probed at point (-7.5, -1.63, 0.11 m); (b) Bistatic RCS for a PEC sphere with a diameter of 15λ

IV. CONCLUSIONS

An effective and stable perfectly matched layer approach has been introduced for DGTD to truncate the computational domain. It applies Discontinuous Galerkin method to both the UPML Maxwell's curl equations and the auxiliary differential equations (ADE). By recording the intermediate results in the updated processes of E-fields and H-fields, the computation time for auxiliary variables in ADE can be reduced greatly within each time step. Moreover, because the auxiliary variables and Riemann flux on each elemental interface are linked together, the UPML scheme is more stable than the well-posed PML, whose auxiliary variables are only dependent on E-fields and H-fields at the same discrete nodes. Some examples demonstrate the effectiveness of UPML, and the proposed method behaves much more stable than the well-posed PML, which is commonly used as PML absorber in DGTD algorithm currently.

REFERENCES

[1] P. Bonnet, X. Perrieres, F. Issac, F. paladian, J. Grando, J. C. Alliot, and J. Fontaine, Finite-Volume Time Domain Method, in Time Domain Electromagnetics. San Diego,CA: Acade Press, 1999, pp. 307-368.

[2] V. Shankar, C. Rowell and W. F. Hall, Unstructured grid-based parallel solver for time-domain maxwell's equations, *Proceedings of the 1997 IEEE Antennas and Propagation Society*, 1997, p. 98-100.

[3] W. F. Hall and A. V. Kabakian, sequence of absorbing boundary conditions for Maxwell's equations, *Journal of Computational Physics*, pp. 140-155, 2004.

[4] T. Xiao and Q. H. Liu, Three-dimensional unstructured-grid discontinuous Galerkin method for Maxwell's equations with well-posed perfectly matched layer, *MICROWAVE AND OPTICAL TECHNOLOGY LETTERS*, vol.46, pp. 459-463, 2005.

[5] T. Lu, W. Cai and P. Zhang, Discontinuous galerkin time-domain method for gpr simulation in dispersive media, *IEEE T Geosci Remote* 43 (2005), no. 1, 72-80.

[6] X. Ji, T. Lu, W. Cai and P. Zhang, Discontinuous galerkin time domain (dgtd) methods for the study of 2-d waveguide-coupled microring resonators, *J Lightwave Technol.* vol. 23, no. 11, pp. 3864-3874, 2005.

[7] G. Cohen and X. Ferrieres, A spatial high-order hexahedral discontinuous Galerkin method to solve Maxwell's equations in time domain, *Journal of Computational Physics*, pp. 340-363, 2006.

[8] A. H. Mohammadian, V. Shankar and W. F. Hall, Computation of electromagnetic scattering and radiation using a time-domain finite-volume discretization procedure, *Computer Physics Communications*, vol.68, pp. 175-196, 1991.

[9] S. D. Gedney, An anisotropic perfectly matched layer absorbing media for the truncation of FDTD lattices, *IEEE Trans. Antennas Propagat.*, vol.44, pp. 1630-1639, 1996.

[10] J. S. Hesthaven and Warburton, Nodal High-Order Methods on Unstructured Grids I. Time-Domain Solution of Maxwell's Equations, *Journal of Computational Physics*, pp. 186-221, 2002.

[11] A. V. Kabakian, Unstructured Grid-Based Discontinuous Galerkin Method for Broadband Electromagnetic Simulations, *Journal of Scientific Computing*, vol.20, 2004.

[12] M. H. Carpenter and C. A. Kennedy, Fourth-Order 2N-Storage Runge-Kulla Scheme, Tech. Rpt. NASA-TM-109112. 1994.

[13] G. Zhao, THE 3-D MULTI-DOMAIN PSEUDOSPECTRAL TIME-DOMAIN METHOD FOR ELECTROMAGNETIC MODELING, Doctor dissertation, Department of Electrical and Computer Engineering, Duke University, 2005.

[14] A. Taflove and S. C. Hagness, *Computational Electrodynamics The Finite-Difference Time-Domain Method* (Third Edition), BOSTON: ARTECH HOUSE, 2005.

[15] S. D. Gedney et al., A Discontinuous Galerkin Finite Element Time Domain Method with PML, *Antennas and Propagation Society International Symposium*, 2008.